ELSEVIER

Contents lists available at ScienceDirect

Polyhedron

journal homepage: www.elsevier.com/locate/poly



X-ray crystallography and electrochemistry reveal electronic and steric effects of phosphine and phosphite ligands in complexes $Ru^{II}(\kappa^4$ -bda) $(PR_3)_2$ and $Ru^{II}(\kappa^3$ -bda) $(PR_3)_3$ (bda = 2,2'-bipyridine-6,6'-dicarboxylato) $^{^{\ \!\!\!\!/}}$



Sima Yazdani ^a, Braden E. Silva ^a, Thomas C. Cao ^a, Arnold L. Rheingold ^b, Douglas B. Grotjahn ^{a,*}

- ^a Department of Chemistry and Biochemistry, 5500 Campanile Drive, San Diego State University, San Diego, CA 92182, United States
- ^b Department of Chemistry and Biochemistry, University of California, San Diego, La Jolla, CA 92093-0385, United States

ARTICLE INFO

Article history: Received 18 September 2018 Accepted 16 December 2018 Available online 27 December 2018

Keywords: Ruthenium Phosphine and phosphite ligands X-ray crystallography DFT Electrochemistry

ABSTRACT

We have examined coordination of PR₃ = triphenylphosphine, triethylphosphine, triisopropyl phosphite, trimethyl phosphite, and 1,3,5-triaza-7-phosphaadamantane (PTA) to the fragment Ru^{II}(bda) to better understand how different phosphine and phosphite ligands influence the electronic and structural properties of the Ru^{II} complexes. PTA and P(OMe)₃ afforded complexes with three phosphorus ligands bound to Ru, with the bda being tridentate (κ^3 -N,N,O) in complexes **4** and **5**; for the other three phosphorus ligands, even in the presence of >2 equiv, only Ru^{II}(κ^4 -bda)(PR₃)₂ species **1–3** were seen. Both experimental and computational methods were used to study the complexes. Steric effects are the main factor determining whether bis- or tris(PR₃) complexes are formed. Cyclic voltammetry studies of the complexes revealed an increase in Ru^{III}(III) potential upon having another phosphorus ligand in the equatorial position. Computational studies predict that the additional phosphine ligand in the equatorial plane of **4** engages in significant orbital mixing with the ruthenium center that results in lower energy bonding as compared to the axial phosphine ligands. This work provides the first evaluation of phosphorus ligand steric and electronic effects on the Ru^{II}(bda) fragment.

© 2018 Elsevier Ltd. All rights reserved.

1. Introduction

Phosphines and phosphites $[P(OR)_3]$ are commonly employed as ancillary ligands for transition metal complexes because of their ability to stabilize low valent metal centers, as well as their ability to fine-tune the stereoelectronic features of their transition metal complexes [1,2].

In recent literature, novel ruthenium complexes supported by the dianionic tetradentate bda ligand (bda = 2,2'-bipyridine-6,6'-dicarboxylate) have been shown to be especially potent for catalytic water oxidation. The chelating nature of the bda ligand along the equatorial plane results in a distorted octahedral geometry in its d⁶ metal complexes, with the remaining two coordination sites situated in a diaxial configuration [3–5]. Therefore, the primary route towards modification of bda-supported complexes is substitution of the diaxial ligands L in Ru(bda)(L)₂. Interest in catalytic

E-mail address: dbgrotjahn@sdsu.edu (D.B. Grotjahn).

properties has inspired the synthesis and characterization of a vast array of $Ru(bda)(L)_2$ complexes with axial ligands L coordinated through N, S, and C atoms [3–5]. To our knowledge, examples of $Ru(bda)(L)_2$ where L = PR_3 have yet to be reported.

In this work, we describe the synthesis and characterization of five Ru^{II}(bda)PR₃ complexes bearing phosphine or phosphite diaxial ligands (Fig. 1, 1–5), and investigate the electronic and steric effects of phosphorus ligands on the backbone bda ligand and structure of Ru complexes. In addition, we attempt to rationalize the preference for phosphorus ligands to occupy a third equatorial position (for instance PTA [2] and trimethyl phosphite) while others are restricted to coordination of only two ligands in the axial positions.

Steric effects of phosphines were quantified by Tolman in 1977 based on the Corey-Pauling-Koltun model of ligand-metal complexes, leading to the proposal of the well-known Tolman cone angle (θ) [1]. Also, the electron donating ability of phosphorus-containing ligands (PR₃) was studied by Tolman's electronic parameter (TEP), defined as the frequency of the A₁ carbonyl mode of (R₃P)Ni (CO)₃ complexes [1]. The steric and electronic profiles of a phos-

^{*} In honor of Bill Jones on his 65th birthday – let there be many more

^{*} Corresponding author.

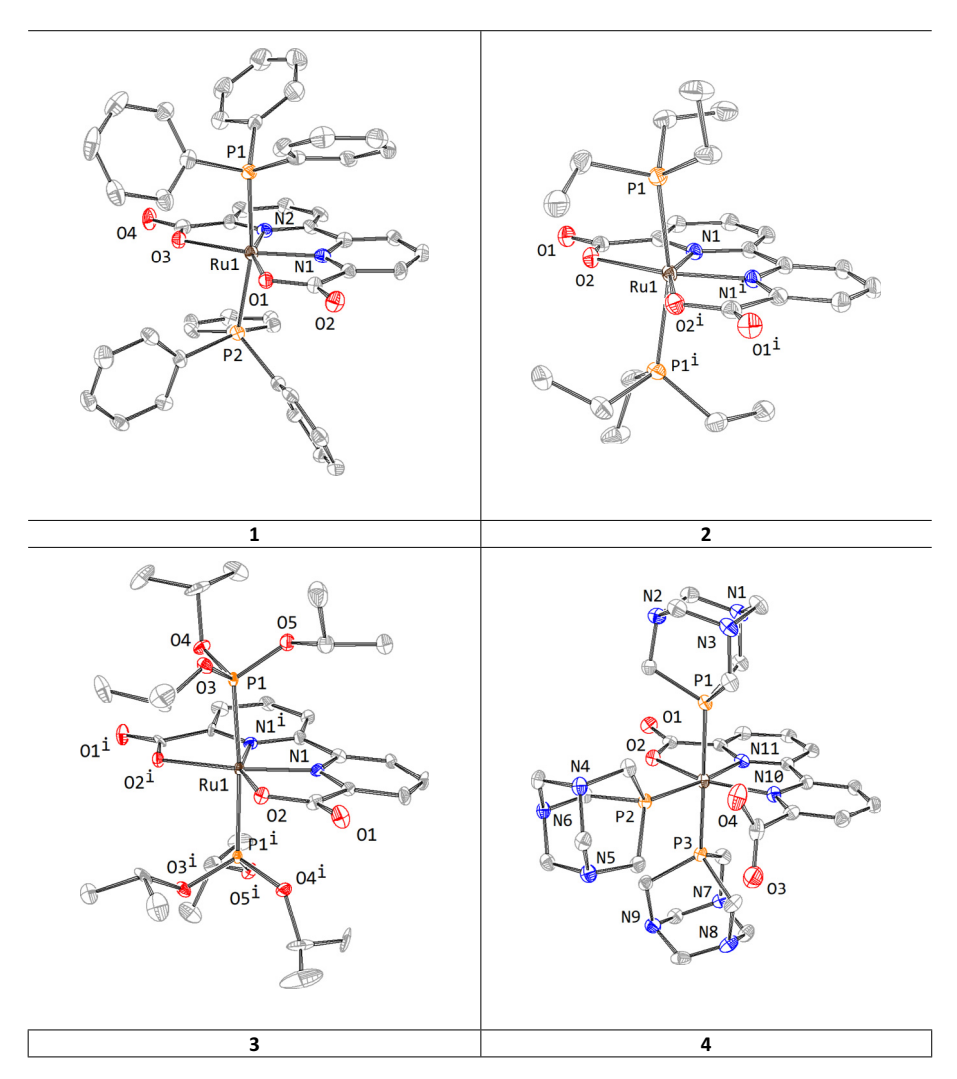


Fig. 1. X-ray crystal structure of complexes 1 to 4. Selected bond lengths [Å] and angles [°] are listed in Table 1.

phine, as measured by θ and TEP, respectively, can impart a significant degree of control over the outcome of transition-metal-mediated reactions. More recent examples of detailed studies on a variety of phosphorus ligands are those of Suresh and co-workers [6,7], who used a combined approach of quantum and molecular mechanics to estimate and separate the steric effects of a PR₃ ligand from its electronic effects. By means of a stereoelectronic plot, one may select ligands as part of designing an organometallic catalyst [2,6]. The electronic effects of substituted phosphines were quantified in terms of the molecular electrostatic potential minimum (V_{\min}) by Suresh and Koga [6,7]. In a recent review, Kühl had compared various methods used for predicting the electronic effects of phosphine ligands and supported the use of (V_{min}) as a parameter for the quantification of electronic effects of phosphine ligands [8]. Therefore, in our work we selected various phosphine and phosphite ligands to examine the electronic and steric effects on $Ru(bda)(PR_3)_n$ complexes (Scheme 1).

2. Materials and methods

2.1. Physical measurements

¹H NMR and ³¹P NMR spectra were taken on Varian 500 MHz Inova or 400 MHz VNMRS NMR spectrometers. Suitable single crystals for X-ray crystallography were grown using vapor diffu-

sion of chloroform into methanolic solutions of complexes **1**, **2**, **3**, and **4**. X-ray crystal structure determinations of complexes were obtained with Bruker single-crystal diffractometers with CCD detectors and low-temperature cryostats with hi-flux Cu and Mo radiation sources. Cyclic voltammetry (CV) measurements were carried out on CH instruments CHI760E and CHI600C potentiostats, with glassy carbon working electrode (diameter – 3 mm), and Pt counter-electrode, with Ag⁺/AgCl reference electrode.

2.2. Synthesis

Synthesis of 6,6'-dimethyl-2,2'-bipyridine: A mixture of Ni(PPh₃)₂-Br₂ (12.95 g, 0.01743 mol), Bu₄NI (21.46 g, 0.05811 mol) and Zn dust (3.81 g, 0.0583 mol) in this order was added to a flask which was then charged with THF (210 mL) and mixture was stirred under N₂ atmosphere at room temperature, after which 2-bromo-6-methylpyridine (10.0 g, 0.0581 mol) was added, and the mixture was refluxed overnight. The solvents were removed by rotary evaporation, and the crude product checked by ¹H NMR. Diethyl ether (200 mL) and 10% NH₄OH (50 mL) were added to the crude reaction and the mixture was stirred for 1 h, after which solids were removed by filtration and purified by column chromatography on silica gel using ethyl acetate and hexane yielding 6,6'-dimethyl-2,2'-bipyridine as a white solid (4.20 g, 60%).

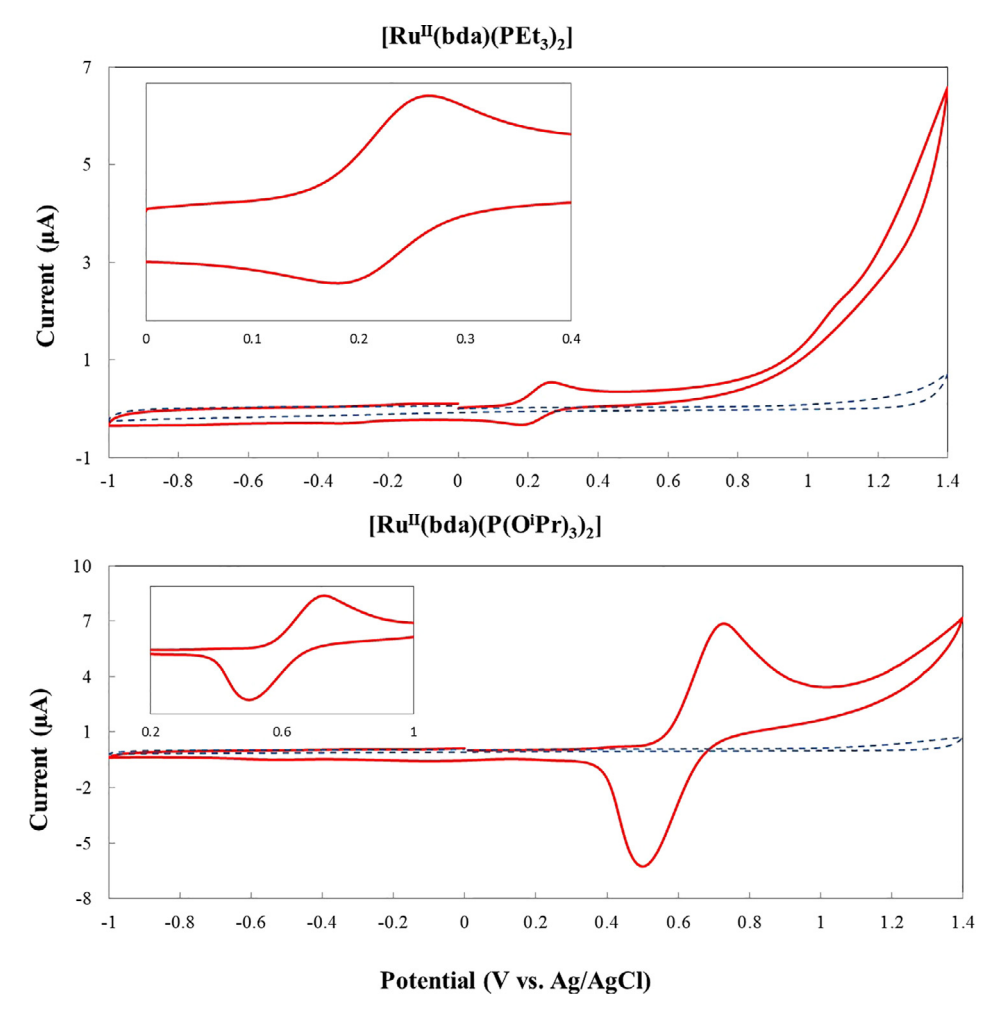


Fig. 2. Cyclic voltammagrams of complexes **2** and **3** (red trace) vs background (in blue) in 0.1 M potassium phosphate buffer/CF₃CH₂OH (4:1) solution (pH 7.0). CV of compound **2** shows $\Delta E_p = 0.0857$ V, forward current = 5.25e–6 A and reverse current = -3.48e-6 A. Compound **3** shows $\Delta E_p = 0.351$ V, forward current = 6.88e-5 A and reverse current = -6.02e-5 A. (Color online.)

Synthesis of 2,2'-bipyridine-6,6'-dicarboxylic acid [5]: The white solid 6,6'-dimethyl-2,2'-bipyridine (4.00 g, 0.0217 mol) was added to concentrated sulfuric acid (80 mL) cooled by an ice bath. Chromium trioxide (13.02 g, 0.1302 mol) was slowly added over 1 h, and the reaction mixture stirred at room temperature for 24 h. Ice was added and the mixture was filtered and the solid washed with water and dry in a vacuum oven (4.76 g, 90 %).

Synthesis of $Ru\ (bda)(dmso)_2$ [5]: Under nitrogen atmosphere a mixture of 2,2'-bipyridine-6,6'-dicarboxylic acid (H₂bda) (1.001 g, 4.099 mmol) and $Ru(dmso)_4Cl_2$ (1.984 g, 4.095 mmol) was added to a 20 mL vial and methanol (5 mL) was added to the vial, followed by Et_3N (0.3 mL), and the mixture refluxed for 24 h. The reaction mixture was allowed to cool, filtered and the solid washed with methanol (20 mL). The product dried under vacuum and the compound was obtained as red-brown solid (1.23 g, 60 %).

Synthesis of Ru (*bda*)(*PPh*₃)₂ (**1**): A 20 mL vial in the glove box was charged with Ru(bda)(dmso)₂ (0.1000 g, 0.1994 mmol) and methanol (2.5 mL) was added. Another vial was charged with triphenylphosphine (0.1046 g, 0.3988 mmol) and methanol (2.5 mL) was added. The two suspensions were mixed together. The resulting mixture sonicated for 1 h, then was stirred overnight. The completion of reaction was verified by 31 P NMR and filtered to give product (0.156 g, 92 %).

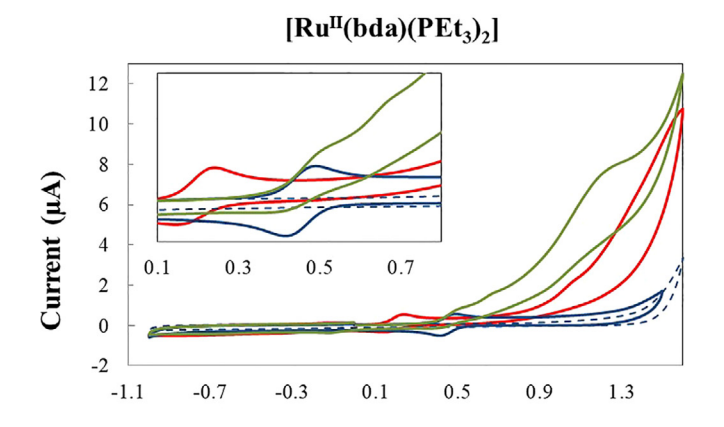
Synthesis of Ru(bda)(PEt₃)₂ (2): The Ru^{II} (bda)(dmso)₂ complex (0.0500 g, 0.0997 mmol) were dissolved in methanol (10 mL) then triethylphosphine (0.0271 mL, 0.2004 mmol) was added. The reac-

tion mixture was stirred 12 h at room temperature. The suspension was filtered, and the brown filtrate solution was concentrated under vacuum. The residue was recrystallized from methanol (0.0348 g, 60%).

Synthesis of $Ru(bda)(P(O^iPr)_3)_2$ (3): Under N_2 atmosphere in a 20 mL vial Ru^{II} (bda)(dmso)₂ (0.050 g, 0.0996 mmol) was added and CH_2Cl_2 (3.5 mL) was added. In a separate vial, triisopropyl phosphite (0.049 mL, 3.988 mmol) was added to CH_2Cl_2 (3.5 mL) and then the solution was added to the content of the other vial. The reaction mixture was stirred for 12 h. The reaction was filtered, and the filtrate was concentrated to dryness and product checked by 1H and ^{31}P NMR (0.0547 g, 72%).

Synthesis of Ru^{II} (bda)(PTA)₃ (**4**): Under N₂ atmosphere to Ru^{II} (bda)(dmso)₂ (0.0311 g, 0.06200 mmol) was added methanol (1 mL). In a separate vial the 1,3,5-triaza-7-phosphaadamantane (0.0342 g, 0.1550 mmol) dissolved in methanol (1.5 mL total amount of methanol) and two precursor solutions were combined and the resulting mixture stirred at room temperature for 0.5 h. The mixture was filtered, and filtered solid was dried under vacuum. The obtained orange solid was washed with methanol (0.5 mL) (0.0475 g, 86%).

Formation of Ru $(bda)(P(OMe)_3)_3$ (5): In the glovebox, a resealable NMR tube was charged with Ru^{II} $(bda)(dmso)_2$ (0.010 g, 0.0199 mmol) and 2 equiv of trimethyl phosphite (0.0047 mL, 0.0399 mmol), then 0.5 mL of CD₃OD, were added and the NMR tube was sealed. Outside the glovebox, the tube was placed in a



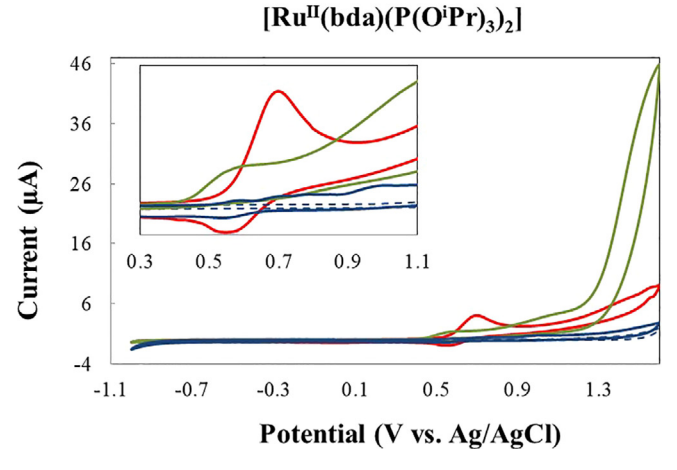


Fig. 3. Comparison of CVs in present of compounds $\bf 2$ and $\bf 3$; blue line pH 1, red line pH 7, and green line pH 10–11 in mixed potassium phosphate/CF $_3$ CH $_2$ OH solution showing two reversible waves of Ru^{III/II} and Ru^{IV/III} redox couples. (Color online.)

rotating oven in 30 °C for 24 h which resulted in a clear yellowish solution containing a combination of **5** and Ru (bda)(dmso)(P (OMe)₃) complexes in 1:1 molar ratio, along with liberated dmso. For comparison, we set up another reaction with excess of tri-

methyl phosphite (0.0070 mL, 0.0598 mmol), which formed **5** and dmso after 2 d in a rotating oven at 30 °C. The complexes were characterized by ¹H and ³¹P NMR data (Table 2) but not isolated.

2.3. Crystal structure determination

Suitable single crystals from the methanol solutions of complexes **1**, **2**, **3**, and **4** were obtained mostly by diffusion technique. Selected crystallography information is presented in Table 1.

3. Results and discussion

3.1. Synthesis and isolation

Reactions for making Ru complexes performed at room temperature afforded high yields (up to 92%). In some cases the crude products were further purified by recrystallization. The reaction of PTA was the fastest, being finished in 0.5 h, whereas the reaction of P(OMe)₃ was the slowest, requiring 2 d to complete.

Complexes **1**, **2**, and **3** were isolated as disubstituted Ru(bda) (L)₂ species. Addition of an excess of phosphorus ligands did not result in trisubstituted complexes analogous to **4**; for example, using 3 equiv of PEt₃, only bis(PEt₃) species **3** and no tris(PEt₃) species could be detected in ¹H and ³¹P NMR spectra (estimated detection limit, 5% yield). In contrast, when making complex **4**, if only 2 equiv of PTA was used, we observed ca. 2/3 of product **4** and unreacted Ru(bda)(dmso)₂ species. Interestingly, when making **5**, if only 2 equiv of P(OMe)₃ was used, we observed both **5** and partially reacted Ru(bda)(dmso)[P(OMe)₃] in a ratio of 1:1.

3.2. NMR and X-ray characterization

Complexes **1–5** were characterized by NMR spectroscopy (Table 2), and complexes **1–4** were isolated and characterized by X-ray crystallography (Table 1 and Fig. 1).

The ¹H NMR spectral data for **1** are illustrative. The signals for bda protons indicate symmetry consistent with tetradentate coordination mode. The spectrum shows one set of resonances for the bda ligand, with each signal representing two protons [8.29 (d),

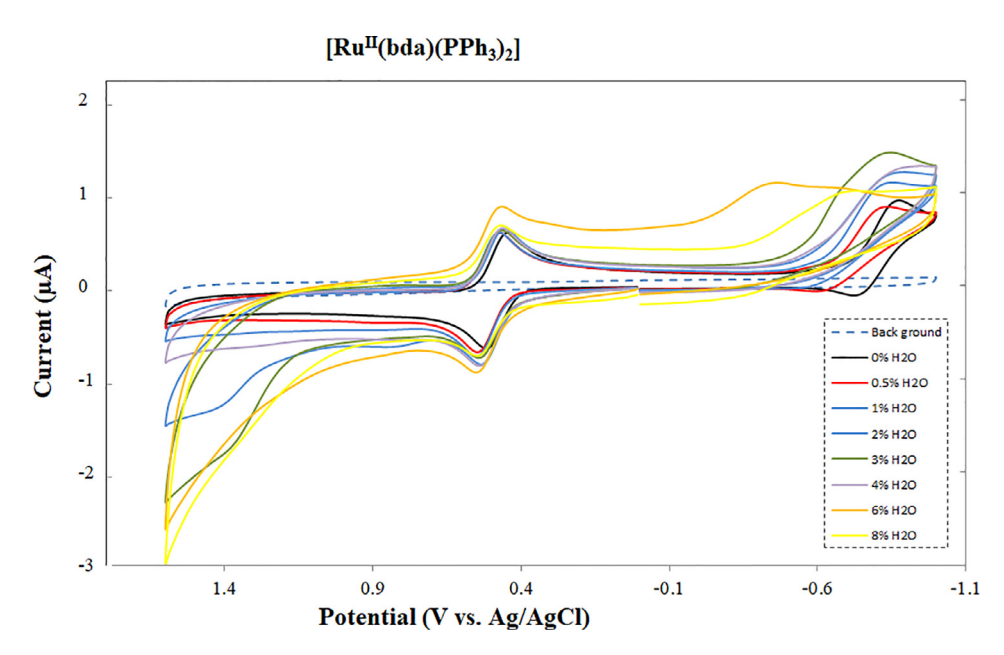


Fig. 4. CVs of 1 mM of 1 in 0.1 M "Bu₄NPF₆/PC by addition of increasing amounts of water, as illustrated in legend of the figure. The dashed line shows the background in the absence of 1.

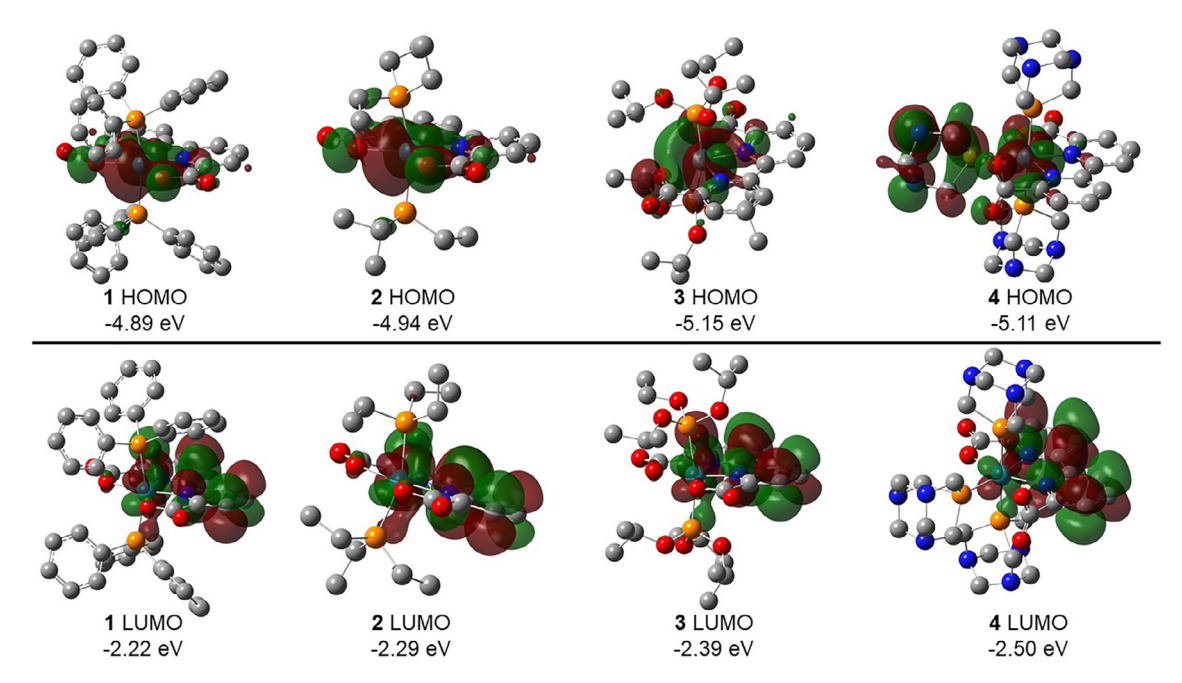
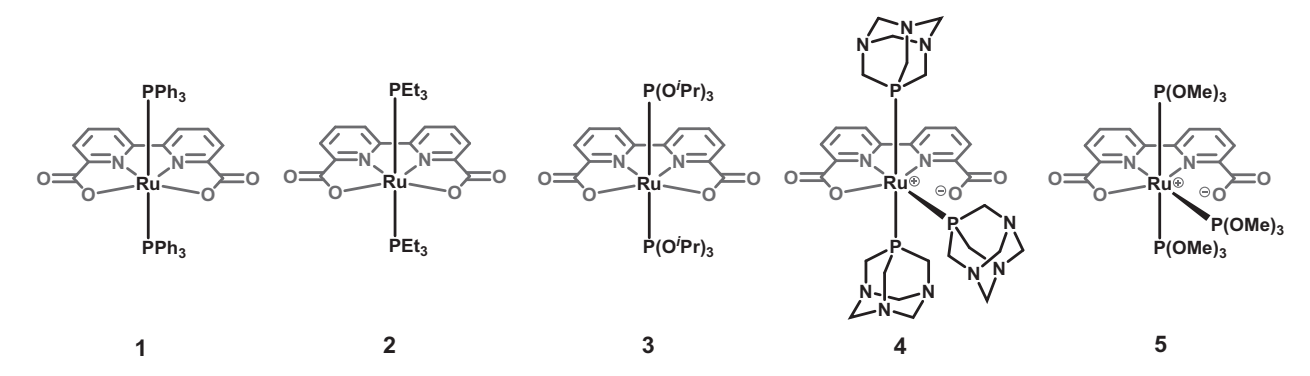


Fig. 5. Selected molecular orbitals for 1 to 4.



Scheme 1. Complexes described in this work.

Table 1 Bond lengths (Å) and angles (°) obtained by X-ray crystallography.

	Complex	1	2	3	4 ^a	4 ^b
Bond lengths (Å)	Ru—O	2.191(3)	2.194(16)	2.208(4)	2.139(15)	-
		2.223(3)	2.194(16)	2.217(6)	_	_
	Ru-N	1.946(4)	1.944(19)	1.986(12)	2.1402(18)	_
		1.954(4)	1.944(19)	1.987(2)	2.0187(17)	_
	Ru—P	2.371(12)	2.372(6)	2.353(4)	2.349(6)	2.322(6)
		2.376(12)	2.372(6)	2.384(4)	2.334(6)	-
Angles (°)	O—Ru—O	124.58(11)	124.05(8)	125.28(15)	=	_
	P—Ru—P	167.16(4)	163.92(3)	164.55(12)	175.98(2)	90.51(2), 91.82(2)
	N-Ru-N	81.22(15)	81.40(11)	80.21(4)	77.01(3)	_
	O-Ru-P	86.03(8)	85.14(5)	86.06(4)	86.92(5)	92.56(4)
		89.31(8)	87.34(4)	89.18(5)	89.70(5)	
	O-Ru-N	77.59(13)	77.28(7)	77.22(11)	156.35(6)	_
		157.83(14)	158.67(7)	157.48(5)	-	-

a = axial ligands; b = equatorial ligand.

8.27 (d), 7.63 (t)], and a multiplet (7.37–7.06 ppm) for the triphenylphosphine axial ligands (Fig. 2a in supporting information).

The ^{31}P NMR data for 1-3 show a single sharp signal, whereas for 4 and 5, a doublet and triplet are seen, consistent with one

unique P coupled to two other, equivalent phosphines. The 1 H NMR data for **4** in CD₃OD (Table 2 and Fig. S4a) are also distinct from those for **1–3**, in that the aromatic region shows six sharp signals instead of only three. In the reaction containing **5** observed in

Table 2 ¹H and ³¹P NMR spectra of compounds **1–5** in CD₃OD.^a

	¹H		³¹ P	
	bda	PR ₃		
1	8.29 (dd, <i>J</i> = 8.0, 1.1, 2H),	7.40–7.30 (m, 6H),	30.8 (s) ^c	
	$7.64 (t, J = 7.8, 2H)^{b}$	7.26-7.13 (m, 14H),		
		7.14–7.05 (m, 12H) ^b		
2	8.43 (dd, J = 8.0, 1.1, 2H),	1.27 (qt, J = 7.5, 2.9, 12H),	16.4 (s)	
	8.15 (dd, J = 7.7, 1.2, 2H),	0.66 (p, J = 7.6, 18H)		
	7.95 (t, J = 7.9, 2H)			
3 d	8.38 (dd, J = 8.0, 1.1, 2H),	4.62-4.56 (m, 6H)	116.5 (s)	
	8.08 (dd, J = 7.8, 1.1, 2H),	1.01 (d, 36H)		
	8.00 (t, J = 7.8, 2H)			
4 e	8.80 (d, J = 8.2, 1H)	4.85, 4.67 (two d, <i>J</i> = 13.1, total 6H)	-51.6 (t) and -55.1 (d) (${}^{2}J_{PPcis} = 38.7$)	
	8.51 (d, J = 8.6, 1H)	4.57 (s, 6H),		
	8.46 (d, J = 8.0, 1H)	4.42, 4.32 (two d, J = 13.1, total 12H), 3.73, 3.60 (two d, J = 15.3, total 12H)		
	8.30 (d, J = 7.6, 1H)			
	8.14 (t, J = 7.8, 1H)			
	7.55 (d, J = 7.9, 1H)			
$5^{\mathrm{d,f}}$	\sim 8.56 (broad, \sim 1H)	3.44 (vt, <i>JN</i> = 10.4, 18H),	136.27 (t) and 121.76 (d) (${}^{2}J_{PPcis} = 68.0$)	
	\sim 8.35 (broad, \sim 1H)	3.92 (d, J = 10.5, 9H)		
	\sim 8.27 (broad, \sim 1H)			
	\sim 8.02 (broad, \sim 2H)			
	\sim 7.51 (broad, \sim 1H)			

(a) Chemical shifts δ in ppm, coupling constants J in Hz. (b) One 2H signal for bda included under signals for PPh₃ ligands. (c) In DMSO- d_6 . (d) In CD₃OD. (e) In CDCl₃. (f) in reaction solution, CD₃OD solvent.

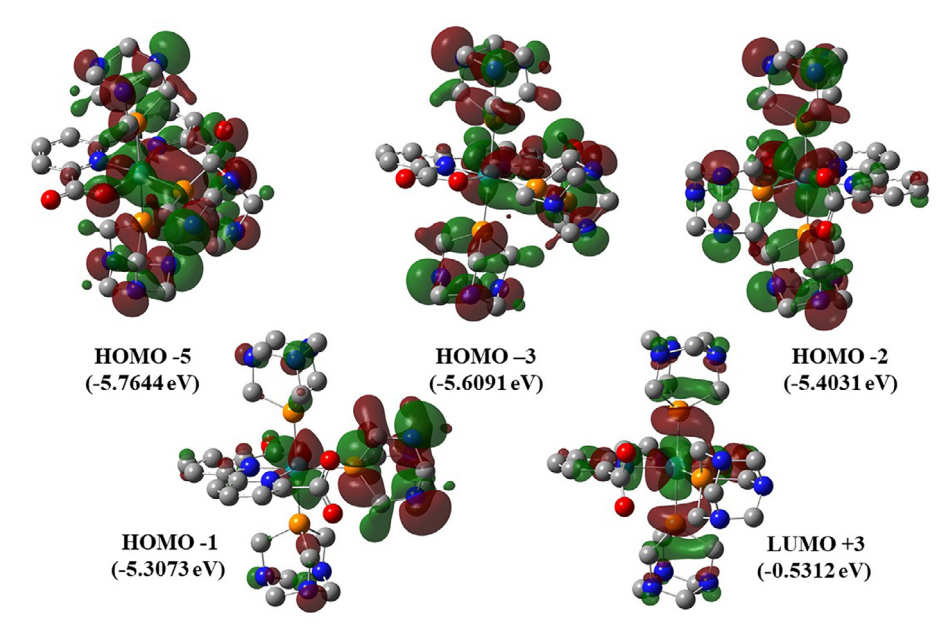


Fig. 6. Selected molecular orbitals for 4.

 CD_3OD solution, the 1H and ^{31}P NMR signals for the non-bda nuclei are sharp (Fig. S5), whereas the 1H NMR signals for the bda protons are broadened, possibly because the protic solvent CD_3OD interacts with the negative charge on the dangling CO_2^- moiety.

The solved X-ray structures revealed that compounds **1**, **2**, and **3** have C_{2v} symmetry, orthorhombic crystal system and Pbcn and Pbca space group with molecular formula Ru(bda)L₂. The complex **4** is monoclinic and C 2/c space group.

As illustrated in Fig. 1, the RuL₂ (Fig. 1a-c) complexes are in a distorted octahedral configuration with N, N, O, O, atoms of bda occupying the equatorial square plane, whereas phosphine and phosphite ligands bound to Ru are in the axial positions. Notably, in complex 4 three PTA ligands are coordinated with the metal center in axial and equatorial positions, forcing one of the carboxylates away from metal center. As may be expected, compound 4 exhibits

different bond lengths and angles compared to compounds **1–3**. The O—Ru—P and P—Ru—P angles are larger in **4** than any of the other reported complexes, on average 1.1° and 10.8°, respectively, and the O—Ru—N (156°) angle is small compared to those of other complexes Also, the Ru—N bonds are longer and Ru—P bonds are shorter in **4** as compared to compounds **1–3**, on average (0.12 Å and 0.03 Å, respectively). Additionally, it is interesting to note that the equatorial Ru—P distance in **4** is on average 0.02 Å shorter than the axial Ru—P bond lengths, likely a result of mutual *trans* influence of the two axially disposed ligands.

The fact that complexes **1–3** were formed exclusively even when excess ligand was present, whereas **4** and **5** appeared to be formed exclusively even when insufficient ligand was present, is rather remarkable. We explain the dichotomous behavior based on the cone angle of phosphorus ligand: the cone angles for PPh₃,

PEt₃, P(OiPr)₃, P(OMe)₃ and PTA are 145°, 132°, 128°, 107° and 103°, respectively [1,2]. In our hands, PTA and P(OMe)₃ gave Ru (bda)L₃ complexes, and these two ligands have the smallest cone angles. In contrast, the electronics of the five phosphine and phosphite ligands (TEP for PEt₃ = 2061.7, PPh₃ = 2068.9, PTA = 2069, P (OiPr)₃ = 2075.9, and P(OMe)₃ = 2079.5 cm⁻¹) [1,2] do not correlate to the reactivity we observe here. Therefore, we conclude that steric effect (as measured by cone angle) determines whether bis- or tris(PR₃) complexes are formed.

However, another way to explain the preference for PTA to coordinate in both axial and equatorial positions it is useful to consider parameters designed to rank steric and electronic properties of phosphine ligands. Based on investigations of Suresh and coworkers [6,7], V_{min} for the ligands PEt₃, PPh₃, PTA, and P(OMe)₃ are -43.55, -34.07, -33.69 and -26.12 kcal/mol, respectively. Phosphines possessing a more negative V_{\min} values are expected to show stronger electron donating properties, while phosphines with less negative V_{\min} values are expected to show more electron-withdrawing properties [6]. Additionally, steric effects of substituents on phosphorus influence the electron donating/ withdrawing effects of the overall phosphine ligand. For example, changes in the bulkiness of substituents attached to phosphorus can alter the p-character of the sp³-hybridized lone pair electrons of the phosphorus atom; which would lead to an overall increase in the V_{\min} value. We note that PPh₃ and PTA have very similar V_{\min} values (and also similar TEP, see previous paragraph), yet here react very differently.

3.3. Electrochemistry

Redox properties of **1–4** were investigated using cyclic voltammetry (CV). CV was first conducted in aqueous potassium phosphate solution (0.1 M, μ = 0.1 and pH 7) (Figs. 2 and S6). A summary of electrochemical results for **1–4** is presented in Table 3. At pH 7 a clearly reversible Ru^{II/III} couple was observed in the CV of **2** and **3**. As shown in Table 3, the redox wave of Ru^{II/III} shows an increasing trend as PEt₃ < PPh₃ < P(OⁱPr)₂ < PTA from 0.25 V to 0.95 V. As we expected, the oxidation potential of compound **4** is higher than that of the other complexes in the series. We attribute this to strong π -interactions between the additional phosphine ligand and the Ru center and to the fact that in complex **4**, the Ru center is formally cationic, whereas in **1–3**, it is neutral.

The coordination chemistry of PTA has been investigated thoroughly [2]; Peruzzini and co-workers suggest that PTA and phosphite ligands are comparable in their σ -bonding and π -bonding abilities. Our electrochemistry data in Table 3 show that $E_{1/2}$ of complex **4** is 0.26 V more positive than $E_{1/2}$ of compound **3** probably because of cationic Ru in the complex **4**.

For further investigation of the redox behavior of these compounds, CV spectra were recorded in mixtures of potassium phosphate buffer/CF₃CH₂OH with three different pH values. Fig. 3 shows the pH dependent behavior of compounds **2** and **3**. An increase in $E_{1/2}$ oxidation peak with increase of pH observed for complex **3**. Furthermore, as shown in Fig. 3 at acidic (blue line)

Table 3 Electrochemical features of 1-4 (0.5 mM) in 0.1 potassium phosphate buffer/CF₃-CH₂OH (4:1) solution (pH 7.0).

Complex	$E_{1/2}^{OX}$ (V vs Ag/AgCl)	
	Ru(II/III)	$E_{ m onset}$
Ru ^{II} (bda)(PPh ₃) ₂	0.45	1.4
Ru ^{II} (bda)(PEt ₃) ₂	0.25	1.2
Ru ^{II} (bda)(P(OiPr) ₃) ₂	0.69	1
Ru ^{II} (bda)(PTA) ₃	0.95	1.1

and basic (green line) pH, two waves are observed, where the second one is smaller and appears at more positive $E_{1/2}$ which may assign for $Ru^{II/III}$ and $Ru^{III/IV}$. For complexes ${\bf 1}$ and ${\bf 4}$ we were not able to perform CV at different pH values because of poor solubilities.

However, the cyclic voltammetry result for complex **1** did not clearly show redox waves for Ru^{II/III} and/or Ru^{III/IV} couples in aqueous solution, possibly because of low solubility in aqueous solvent. We investigated propylene carbonate (PC) as a polar aprotic solvent to solubilize complex **1** during the electrochemistry experiments [9]. Fig. 4 illustrates the cyclic voltammograms of 1 mM **1** in 0.1 M $^{0.1}$ M $^{0.1}$ M $^{0.1}$ M $^{0.1}$ W in the absence of water and in presence of water clearly a wave is observed at $E_{1/2} = 0.45$ V for redox of Ru^{III/II}. In fact, after adding water, the potential of the II/III couple did not change [9].

3.4. DFT computations

All molecular structures were optimized in the *Gaussian16* Revision D.01 [10] program with the B3LYP density functional [11–13] with the cc-pVDz basis set [13] for all main group atoms and the Stuttgart–Dresden (SDD) [13–15] effective core potential for ruthenium. All stationary points were verified by frequency calculations and full population analysis. All calculations were carried out on isolated gas-phase species.

To aid in our study of these $Ru^{II}(bda)(PR_3)_2$ complexes, we investigated the calculated molecular orbitals in order to probe the extent of bonding interactions between Ru and the PR_3 ligands. We initially began by optimizing the set of isolated compounds **1–4**, as well as species not observed experimentally, complexes corresponding to **1–3** containing an additional phosphine ligand in the equatorial plane with an unbound carboxylate, and the complex $Ru^{II}(\kappa^4$ -bda)(PTA)₂ where both bda carboxylates are bound to ruthenium. However, we were unable to locate a minimized structure of the type $Ru^{II}(\kappa^3$ -bda)(PR₃)₃ when PR₃ is PPh₃, PEt₃, or P(OiPr)₃, which we attributed to unfavorable steric interactions.

Orbital analysis of compounds 1-3 reveal similar bonding features, including the highest occupied molecular orbitals (HOMO) being centered on carboxylate oxygens and the ruthenium center with σ -symmetry, and lowest unoccupied orbitals being mainly located on the bipyridine moiety of the bda (Figs. 5 and 6, Table 4). Comparing complexes 1-3 of similar structure, the HOMO-LUMO gap for compound **3** was found to be bigger than other complexes) (Table 4) which can be rationalized by P(OiPr)₃ having the largest TEP value (2075.9 cm $^{-1}$) (Table 4). Turning now to compound 4, analysis showed the HOMO to be a σ -interaction between bda nitrogens and ruthenium, as well as PTA orbitals. The LUMO was again mainly centered on the bipyridine part of the bda ligand, however in this case showing some π anti-bonding character between bda nitrogens and ruthenium. Analysis of lower energy orbitals in compound 4 (Figs. 4 and 5) show low energy (HOMO -5 and HOMO -3) orbitals with π -bonding character between the equatorial PTA and ruthenium. Interestingly, the HOMO -2orbital shows π anti-bonding character between the axial PTA ligands and ruthenium, as well as some density on the equatorial

Table 4 Computed HOMO–LUMO gaps for $Ru^{II}(bda)(L)_{2,3}$ species (this work) and Tolman electronic parameters for L (literature [1]).

Complex	HOMO/LUMO gap (eV)	PR ₃ TEP (cm ⁻¹)
1, Ru ^{II} (bda)(PPh ₃) ₂	2.669	2068.9
2, Ru ^{II} (bda)(PEt ₃) ₂	2.653	2061.7
3, $Ru^{II}(bda)(P(OiPr)_3)_2$	2.760	2075.9
Ru ^{II} (bda)(PTA) ₂	2.656	2069
4 , Ru ^{II} (κ^3 -bda)(PTA) ₃	2.613	

PTA, however in this case with non-bonding character with respect to the ruthenium. The HOMO -1 orbital is π anti-bonding in character between the equatorial PTA and ruthenium. Overall, there is a net π bonding interaction between the equatorial PTA ligand and the ruthenium, which also may help explain the favorability of three PTA ligands to coordinate.

4. Conclusions

Here we report synthesis of Ru⁻based complexes using the 2,2'bipyridine-6-6'-dicarboxylic acid scaffold. In this work we used one triarylphosphine, one trialkylphosphine, two phosphites, and the unique ligand PTA, each presenting a different combination of steric and electronic effects. For complexes 1 to 3, phosphine and phosphite ligands occupy the two axial coordination sites available on the fragment Ru(κ^4 -bda). In contrast, complexes **4** and 5 possess an additional phosphine ligand occupying the equatorial position, displacing a carboxylato of bda, resulting in Ru(κ^3 bda)(L)₃. Notable is that P(OMe)₃ and P(OiPr)₃ are similar electronically, but the larger steric demand of the latter results in an L₂ complex; similarly, PTA and PPh3 are similar electronically, but the larger steric demand of latter results in an L₂ complex. Moreover, P(OMe)₃ is less electron-rich than PTA and seems to react more slowly (2 d vs. 0.5 h) with Ru(bda)(dmso)₂, but the two ligands share similar cone angles and both give L₃ complexes as final products, where the presumed L₂ intermediate is not detected during reaction.

Comparison of the redox potentials for the II/III couple in Ru (bda)(PR₃)₂ reflects the donor abilities of PEt₃ (0.25 V), PPh₃ (0.45 V) and P(OiPr)₃ (0.69 V). The II/III redox potential for the tris(PTA) complex was more positive, likely because the Ru center bears a formal positive charge thanks to ionization of the Ru–carboxylate bond enforced by the presence of the third, equatorial phosphine. Computational scrutiny of 4 suggests that there is a net π bonding interaction between the equatorial PTA ligand and the ruthenium, which also helps explain the relatively positive potential of the II/III couple.

This work reports the first complexes of phosphorus ligands on the $\mbox{Ru}^{II}(\mbox{bda})$ fragment and points to future exploration of reactivity.

Acknowledgements

We thank San Diego State University for initial support of this work. The later portions of this research were supported by the U.S. Department of Energy, Office of Science, Office of Basic Energy Sciences, under Award DE-SC0018310. Special thanks to Dr. Diane K. Smith for invaluable help with electrochemical methods and Aaron Nash and Daniel Sattler for support during this work.

Appendix A. Supplementary data

CCDC 1868484–1868487 contains the supplementary crystallographic data for **1–4**. These data can be obtained free of charge via http://www.ccdc.cam.ac.uk/conts/retrieving.html, or from the Cambridge Crystallographic Data Centre, 12 Union Road, Cambridge CB2 1EZ, UK; fax: (+44) 1223–336-033; or e-mail:

deposit@ccdc.cam.ac.uk. Supplementary data to this article can be found online at https://doi.org/10.1016/j.poly.2018.12.033.

References

- [1] (a) C.A. Tolman, Steric effects of phosphorus ligands in organometallic chemistry and homogeneous catalysis, Chem. Rev. 77 (1977) 313;
 - (b) C.A. Tolman, Electron donor-acceptor properties of phosphorus ligands. Substituent additivity, J. Am. Chem. Soc. 92 (1970) 2953.
- [2] (a) For reviews about PTA see: J. Bravo, S. Bolaño, L. Gonsalvi, M. Peruzzini, Coordination chemistry of 1,3,5-triaza-7-phosphaadamantane (PTA) and derivatives. Part II. The quest for tailored ligands, complexes and related applications Coord. Chem. Rev. 254 (2010) 555;
 - (b) A.D. Phillips, L. Gonsalvi, A. Romerosa, F. Vizza, M. Peruzzini, Coordination chemistry of 1,3,5-triaza-7-phosphaadamantane (PTA): transition metal complexes and related catalytic, medicinal and photoluminescent applications, Coord. Chem. Rev. 248 (2004) 955;
 - (c) A. Guerriero, M. Peruzzini, L. Gonsalvi, Coordination chemistry of 1,3,5-triaza-7-phosphatricyclo [3.3.1.1]decane (PTA) and derivatives. Part III. Variations on a theme: novel architectures, materials and applications, . Coord. Chem. Rev. 355 (2018) 328;
 - (d), Selected references: J.R. DeLerno, L.M. Trefonas, M.Y. Darensbourg, R.J. Majeste, Molecular structure and spectral properties of phosphatriazaadamantanemolybdenum pentacarbonyl complex Inorg. Chem. 15 (1976) 816:
 - (e) D.J. Darensbourg, J.B. Robertson, D.L. Larkins, J.H. Reibenspies, Water-soluble organometallic compounds. 7. Further studies of 1,3,5-triaza-7-phosphaadamantane derivatives of group 10 metals, including metal carbonyls and hydrides, Inorg. Chem. 38 (1999) 2473;
 - (f) R. Huang, B.J. Frost, Development of a series of P(CH₂N=CHR)₃ and trisubstituted 1,3,5-triaza-7-phosphaadamantane ligands, Inorg. Chem. 46 (2007) 10962:
 - (g) S.N. Britvin, A. Lotnyk, Water-soluble phosphine capable of dissolving elemental gold: the missing link between 1,3,5-triaza-7-phosphaadamantane (PTA) and Verkade's ephemeral ligand, J. Am. Chem. Soc. 137 (2015) 5526;
 - (h) F. Battistin, G. Balducci, E. Iengo, N. Demitri, E. Alessio, Neutral 1,3,5-triaza-7-phosphaadamantane-ruthenium(II) complexes as precursors for the preparation of highly water-soluble derivatives, Eur. J. Inorg. Chem. 17 (2016) 2850;
 - (I) A. Rossin, L. Gonsalvi, A.D. Phillips, O. Maresca, A. Lledós, M. Peruzzini, Water-assisted H-H bond splitting mediated by [CpRu(PTA)₂CI] (PTA = 1,3,5-triaza-7-phosphaadamantane). A DFT analysis, Organometallics 26 (2007) 3289.
- [3] L. Wang, L. Duan, B. Stewart, M. Pu, J. Liu, T. Privalov, L. Sun, Toward controlling water oxidation catalysis: tunable activity of ruthenium complexes with axial imidazole/DMSO ligands, J. Am. Chem. Soc. 134 (2012) 18868.
- [4] J.D. Blakemore, R.H. Crabtree, G.W. Brudvig, Molecular catalysts for water oxidation, Chem. Rev. 115 (2015) 12974.
- [5] L. Duan, F. Bozoglian, S. Mandal, B. Stewart, T. Privalov, A. Llobet, L. Sun, A molecular ruthenium catalyst with water-oxidation activity comparable to that of photosystem II, Nat. Chem. 4 (2012) 418.
- [6] J. Mathew, T. Thomas, C.H. Suresh, Quantitative assessment of the stereoelectronic profile of phosphine ligands, Inorg. Chem. 46 (2007) 10800.
- [7] C.H. Suresh, N. Koga, Quantifying the electronic effect of substituted phosphine ligands via molecular electrostatic potential, Inorg. Chem. 41 (6) (2002) 1573.
- [8] O. Kühl, Predicting the net donating ability of phosphines do we need sophisticated theoretical methods?, Coord Chem. Rev. 249 (5–6) (2005) 693.
- [9] Z. Chen, J.J. Concepcion, H. Luo, J.F. Hull, A. Paul, T.J. Meyer, Nonaqueous catalytic water oxidation, J. Am. Chem. Soc. 132 (2010) 17670.
- [10] M.J. Frisch, G.W. Trucks, H.B. Schlegel, G.E. Scuseria, M.A. Robb, J.R. Cheeseman, G. Scalmani, V. Barone, G.A. Petersson, H. Nakatsuji, X. Li, M. Caricato, et al., Gaussian 16, Revision B.01, Gaussian Inc, Wallingford CT, 2016.
- [11] C. Lee, W. Yang, R.G. Parr, Development of the Colle-Salvetti correlation-energy formula into a functional of the electron density, Phys. Rev. B 37 (1988) 785.
- [12] A.D. Becke, Density-functional thermochemistry. III The role of exact exchange, J. Chem. Phys. 98 (1993) 5648.
- [13] T.H. Dunning, Gaussian basis sets for use in correlated molecular calculations. I. The atoms boron through neon and hydrogen, J. Chem. Phys. 90 (1989) 1007.
- [14] D. Andrae, U. Häußermann, M. Dolg, H. Stoll, H.T. Preuß, Energy-adjusted ab initio pseudopotentials for the second and third row transition elements, Theor. Chim. Acta 77 (1990) 123.
- [15] P. Fuentealba, H. Preuss, H. Stoll, L. Von Szentpály, A proper account of corepolarization with pseudopotentials: single valence-electron alkali compounds, Chem. Phys. Lett. 89 (1982) 418.